Imaging the mantle beneath Iceland using integrated seismological techniques

Richard M. Allen,[1,2] Guust Nolet,[1] W. Jason Morgan,[1] Kristín Vogfjörd,[3] Bergur H. Bergsson,[3] Pálmi Erlendsson,[3] G. R. Foulger,[4] Steinunn Jakobsdóttir,[3] Bruce R. Julian,[5] Matt Pritchard,[4] Sturla Ragnarsson,[3] and Ragnar Stefánsson[3]

Received 25 April 2001; revised 9 April 2002; accepted 23 April 2002; published 6 December 2002.

[1] Using a combination of body wave and surface wave data sets to reveal the mantle plume and plume head, this study presents a tomographic image of the mantle structure beneath Iceland to 400 km depth. Data comes primarily from the PASSCAL-HOTSPOT deployment of 30 broadband instruments over a period of 2 years, and is supplemented by data from the SIL and ICEMELT networks. Three sets of relative teleseismic body wave arrival times are generated through cross correlation: *S* and *SKS* arrivals at 0.03–0.1 Hz, and *P* and *PKIKP* arrivals at 0.03–0.1 and 0.8–2.0 Hz. Prior to inversion the crustal portion of the travel time anomalies is removed using the crustal model ICECRTb. This step has a significant effect on the mantle velocity variations imaged down to a depth of ~250 km. Inversion of relative arrival times only provides information on lateral velocity variations. Surface waves are therefore used to provide absolute velocity information for the uppermost mantle beneath Iceland. The average wave number for the Love wave fundamental mode at 0.020 and 0.024 Hz is measured and used to invert for the average *S* velocity. Combination of the body wave and surface wave information reveals a predominantly horizontal low-velocity anomaly extending from the Moho down to ~250 km depth, interpreted as a plume head. Below the plume head a near-cylindrical low-velocity anomaly with a radius of ~100 km and peak V_P and V_S anomalies of −2% and −4%, respectively, extends down to the maximum depth of resolution at 400 km. Within the plume head, in the uppermost mantle above the core of the plume, there is a relatively high velocity with a maximum V_P and V_S anomaly of +2%. This high-velocity anomaly may be the result of the extreme degree of melt extraction necessary to generate the thick (46 km) crust in central Iceland. Comparison of the plume volumetric flux implied by our images, the crustal generation rate, and the degree of melting suggested by rare earth element inversions, suggests that (1) mantle material must be flowing horizontally away from the plume core faster than the overlying lithosphere and (2) the bulk of the plume material does not participate in melting beneath Iceland. *INDEX TERMS:* 7218 Seismology: Lithosphere and upper mantle; 7203 Seismology: Body wave propagation; 7255 Seismology: Surface waves and free oscillations; 8121 Tectonophysics: Dynamics, convection currents and mantle plumes; *KEYWORDS:* Iceland, mantle structure, plume, tomographic imaging, body waves, surface waves

Citation: Allen, R. M., et al., Imaging the mantle beneath Iceland using integrated seismological techniques, *J. Geophys. Res.*, *107*(B12), 2325, doi:10.1029/2001JB000595, 2002.

1. Introduction

[2] Since its introduction by *Morgan* [1971], the mantle plume hypothesis has been tested by many investigators against geophysical and geochemical observations. Despite occasional opposition, even in recent times [*Anderson*, 2000; *Foulger et al.*, 2000], it is widely accepted that mantle plumes are responsible for hot spot formation. Iceland represents a classic example of such a hot spot located at the center of gravity, bathymetry and geochemical anomalies. As a result, the mantle beneath Iceland has been investigated extensively.

[3] Several seismic tomography images of the uppermost mantle from regional (land-based) networks show a low-velocity anomaly extending to at least the depth of resolution at around 400 km [*Tryggvason et al.*, 1983; *Wolfe et al.*, 1997; *Foulger et al.*, 2000]. While most interpret this anomaly as the top of a high-temperature plume, proof of

[1]Department of Geosciences, Princeton University, Princeton, New Jersey, USA.
[2]Now at Department of Geology and Geophysics, University of Wisconsin-Madison, Madison, Wisconsin, USA.
[3]Vedurstofa Íslands, Reykjavik, Iceland.
[4]Department of Geological Sciences, University of Durham, Durham, UK.
[5]U.S. Geological Survey, Menlo Park, California, USA.

0148-0227/02/2001JB000595$09.00

the plume hypothesis requires evidence of a high-temperature conduit extending through the entirety of the mantle. This evidence comes from a variety of other studies. Receiver functions can be used to map variations in the thickness of the transition zone beneath Iceland, which is related to the temperature of mantle material at these depths. In central and southern Iceland the transition zone is ~20 km thinner than surrounding areas [*Shen et al.*, 1998, 2002], suggesting the high-temperature conduit in the upper mantle extends to at least 660 km. Evidence for a low-velocity, high-temperature conduit in the lower mantle is more ambiguous. *Bijwaard and Spakman* [1999] use the reprocessed International Seismological Centre travel time data set [*Engdahl et al.*, 1998] and an irregular grid parameterization to obtain a three-dimensional (3-D) global *P* velocity model in which they image a low-velocity region beneath Iceland extending to the core-mantle boundary (CMB). A similar structure is recovered by *Zhao* [2001]. However, *Ritsema et al.* [1999], combining surface wave phase velocities, body wave travel times, and free-oscillation splitting measurements, obtain a global *S* velocity model which suggests that the low-velocity anomaly is limited to the upper mantle. Finally, *Helmberger et al.* [1998] have identified an ultralow-velocity zone at the base of the mantle, which they interpret as the plume source. By modeling shear wave phases transmitted through, and refracted at, the CMB they find a 250-km-wide, 40-km-high dome containing *P* and *S* velocity reductions of 10% and 30%, respectively. This is interpreted as indicative of high temperatures and partial melt in D″ at the base of the Iceland mantle plume.

[4] Superimposed on the plume-related processes in Iceland is the Mid-Atlantic Ridge. For the most part, mid-ocean ridges are passive features where mantle material upwells in response to the parting of tectonic plates above. In the case of Iceland, however, the co-location of a mantle plume and ridge results in a non-passive rift zone. Plumes clearly have a significant influence on ridges, as illustrated by the bathymetry and crustal thickness anomalies in the North Atlantic. Also mantle plumes located off mid-ocean ridges continue to influence crustal formation processes up to 1400 km away [*Ribe*, 1996]. Laboratory and numerical models suggest material is fed from the plume to the ridge along sublithospheric pipes [*Kincaid et al.*, 1995; *Ribe*, 1996] though there is no seismological evidence for this.

[5] When the plume is directly beneath the ridge, either all plume material is absorbed into newly formed lithosphere, or sublithospheric material must flow away from the hot spot (i.e. the surficial expression of the plume beneath). We refer to the existence of such a plume-fed asthenospheric layer as the plume head. Tomographic imaging of several plumes has thus far been unsuccessful in identifying such a plume head.

[6] The location of the Iceland plume beneath the North-Atlantic Mid-Ocean Ridge is unlikely to be a coincidence. The most active rift on Iceland today is located directly above the core of the mantle plume and is offset by more than 200 km to the east of the oceanic rifts to the north and south. The exposed Icelandic crust contains evidence of three rift jumps over the last 15 Myr [*Hardarson et al.*, 1997], each moving the rift further east, presumably to remain over the plume, another indication of significant plume-ridge interaction.

[7] The uppermost mantle, where plume-ridge interaction takes place, lies in a depth range for which we have only limited resolving power. Wide-angle seismic studies on Iceland provide detailed structural information about the upper crust and constraints on crustal thickness along their 2-D sections [*Bjarnason et al.*, 1993; *Staples et al.*, 1997; *Darbyshire et al.*, 1998; *Menke et al.*, 1998; *Weir et al.*, 2001]. However, information about deeper structure is so far mostly provided by teleseismic body wave studies. While resolution is good to depths of 400 km, the vertical resolution degrades in the upper ~100 km as rays become more parallel. This results in vertical smearing of velocity anomalies, causing crustal and uppermost mantle anomalies to be mixed in tomographic images.

[8] Here we present the results of a mantle tomographic study using data from regional networks in Iceland, primarily the recent HOTSPOT experiment [*Allen et al.*, 2002]. As with all tomographic studies of Iceland using regional data sets, our resolution deteriorates below ~400 km making it impossible to determine the source depth of the low-velocity anomaly imaged in the upper 400 km. Here we focus on the uppermost mantle beneath the crust, a region where the vertical resolution of previous studies is poor. Through the combination of surface wave phase measurements with the more traditional teleseismic arrival time differences, we are able to recover absolute velocity anomalies rather than relative variations. In addition, we use the crustal model of *Allen et al.* [2002] to correct body wave arrival times for the crustal portion of their paths. The result is a successful separation of crustal and uppermost mantle velocity anomalies, allowing visualization of mantle interaction with the crust in and around this ridge-centered mantle plume.

2. Useful Data

2.1. Seismic Networks

[9] We use a total of 78 seismic stations in our study from the HOTSPOT, SIL, and ICEMELT networks, Figure 1. The HOTSPOT network, circles on Figure 1, was a temporary PASSCAL deployment of 30 broadband instruments (primarily Guralp CMG3-ESP instruments) recording continuous data streams at 20 samples per second from July 1996 till July 1998. *Allen et al.* [2002] includes a description of the deployment. In addition, we use 33 stations from the Southern Iceland Lowlands project (SIL network), which provided useful teleseismic body wave arrivals during the period of the HOTSPOT deployment. This permanent network operated by Vedurstofa Íslands is a mixture of short-period and broadband instruments [*Stefansson et al.*, 1993] shown as open and solid triangles, respectively, on Figure 1. In addition, the ICEMELT experiment deployed five broadband instruments from 1993 to 1994, and an additional 10 instruments in the spring of 1995, all 15 operated until 1996. All were Streckeisen STS-2 instruments belonging to the Carnegie Institution of Washington. They recorded continuously at 10 samples per second [*Bjarnason et al.*, 1996] and are shown as squares on Figure 1. Event data from this network were retrieved through the IRIS-DMC. Approximately 65% of the data come from the HOTSPOT network, ICEMELT provides most of the additional low-

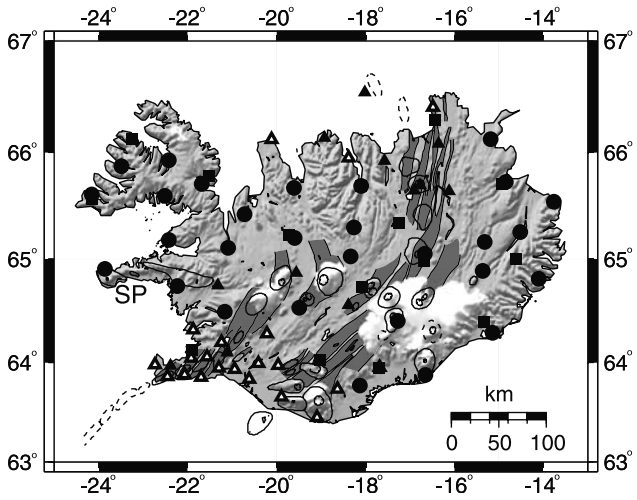

Figure 1. Seismic stations used in the mantle body wave study. These come from three networks: the HOTSPOT (circles) and ICEMELT (squares) networks, both consisting of broadband instruments, and the SIL network consisting of broadband (solid triangles) and short-period (open triangles) instruments. SP indicates the Snæfellsnes Peninsula referred to in the text.

frequency data, and SIL provides mainly high-frequency data.

2.2. Frequency Windows

[10] *Allen et al.* [1999] demonstrated that the data quality of the portable HOTSPOT network is comparable to that of the permanent borehole Global Seismic Network station BORG. However, all stations on Iceland suffer relatively high levels of microseismic noise due to their close proximity to the stormy North Atlantic. There is a single noise peak at 0.25 Hz [see *Allen et al.*, 1999, Figure 3] making picking or cross correlation of arrivals impossible for all but the largest events at this frequency. Therefore we use arrivals in frequency windows above and below the microseismic noise peak in this study. *P* and *PKIKP* are picked and cross-correlated in two frequency windows: 0.03–0.1 and 0.8–2.0 Hz, while *S* and *SKS* are only observed in the lower-frequency window. We expect the best resolution of mantle anomalies from the high-frequency *P* and *PKIKP* arrivals, but the lower-frequency V_P model is also useful for comparison with the low-frequency V_S model.

2.3. Teleseismic Earthquakes

[11] The teleseismic body wave travel time data set used here is derived from inspection of waveforms at all available stations for 942 teleseismic earthquakes. We generated event gathers from HOTSPOT and SIL data for all magnitude $\geq$6.0 earthquakes, and earthquakes with magnitude $\geq$5.4 at epicentral distances $\leq$100°, during the duration of the HOTSPOT experiment (July 1996 to July 1998). In addition, we used all earthquakes recorded on five or more of the ICEMELT stations that met the same magnitude and epicentral distance criteria. The 300 earthquakes providing useful data for this study are shown in Figure 2a. The proportion of useful earthquakes as a function of magnitude is shown in Figure 2b. In this study we use the PDE earthquakes locations provided by the National Earthquake Information Center.

[12] Table 1 shows the percentage of events providing useful data during the course of the HOTSPOT deployment. There is also a significant seasonal variation in the number of useful events due to the higher noise levels on Iceland in the winter months. For events with magnitudes $\geq$6.0 within 90° of Iceland, there was a 40% increase in the number of useful events between the winter (January–April) and summer (June–August).

3. Body Wave Processing and Inversion

[13] The responses of the broadband instruments used in this study are flat for velocity across our two frequency windows. In order to accommodate the short-period SIL instruments in the high-frequency data set, we transform all HOTSPOT and SIL data to the response of the shortest-period instrument, a Lennartz-1, thus providing comparable

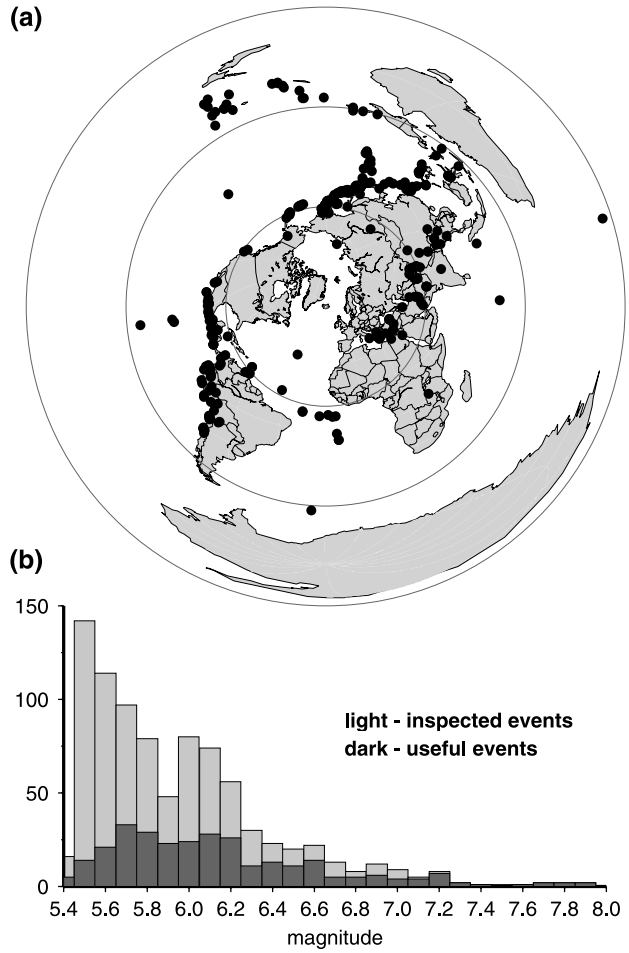

Figure 2. (a) Distribution of the 300 earthquakes used in the body wave study providing *P*, *PKIKP*, *S*, and *SKS* phases with an excellent azimuthal coverage. (b) Histogram comparing the number of earthquakes (light gray) to the number providing useful data (dark gray) as a function of magnitude. There were 40% more useful earthquakes in the summer months than in the winter.

Table 1. Number of Events Providing Useful Data for Different Phases and Frequency Windows[a]

Event Criteria	Number of Events	Percent Providing Useful Data	Percent Providing Useful Shear Phases	Percent Providing Useful Low-Frequency Compressional Phases	Percent Providing Useful High-Frequency Compressional Phases
mag $\geq$ 6.0, $\Delta \leq 90°$	158	70	38	45	46
$5.5 \leq$ mag $\leq$ 5.9, $\Delta \leq 90°$	381	28	9	12	15
mag $\geq$ 6.0, *SKS*	196	24	24		
mag $\geq$ 6.0, *PKIKP*	126	22		18	14

[a]The statistics are calculated using all events during the 2-year deployment of the HOTSPOT network.

waveforms for each event and allowing consistent picking and cross correlation.

3.1. Cross Correlation

[14] We use the cross-correlation approach of *VanDecar and Crosson* [1990] to optimize the quality of our travel time delays. The pick is only used to select a time window for cross correlation around the arrival, while the length of the window was selected for each event to include one to a few cycles. Cross correlation was performed for each phase in each of our frequency windows to obtain relative arrival times, Δt_{ij}, between all pairs of stations i, j. The relative travel time for each station, t_i, is then obtained by minimizing the residual, res_{ij}, defined as

$$\text{res}_{ij} = \Delta t_{ij} - (t_i - t_j) \tag{1}$$

for all station pairs. With the addition of the constraint that $\Sigma \Delta t_i = 0$ this system is solved. After correcting for the variation in epicentral distance using the 1-D Earth model IASP91 we obtain a "relative" travel time data set sampling the 3-D heterogeneity's beneath Iceland. The consequence of this approach is the loss of absolute travel time, preventing recovery of velocity anomalies (with respect to IASP91) common to all ray paths. Far away from Iceland, small anomalies will effectively heal [*Nolet and Dahlen*, 2000], while large anomalies affect the travel time along each ray similarly and the delay cannot be distinguished from a source correction. However, even beneath Iceland our data are insensitive to a constant velocity perturbation in a layer of constant thickness because the rays travel virtually parallel through this layer. In section 4 we show, however, that absolute information on S velocity can be obtained from surface waves.

[15] In addition to providing consistent and accurate travel time measurements, cross correlation also allows a formal assessment of the error associated with each arrival based on the residuals. The standard deviation σ_i for the distribution of arrival time t_i is

$$\sigma_i = \sqrt{\frac{1}{\gamma} \sum_{j \neq i} \text{res}_{ij}^2}, \tag{2}$$

where i and j again represent pairs of the n stations. The choice of γ is dependent on the degree to which estimates of travel time measurement error, using cross-correlation residuals, are considered to be independent. If they are considered to be independent for each station, as would be the case for a random signal perturbation, γ should be set to $(n - 1)(n - 2)$. If, however, they are dependent as suggested by *VanDecar and Crosson* [1990], a γ of $(n - 2)$ would be more appropriate. The true value probably lies between these two estimates so we quote both to indicate the possible range of errors. The end-member estimates of the average standard deviations for our travel time data sets are 0.05–0.25 s, 0.04–0.20 s, and 0.02–0.10 s for the shear, low-frequency and high-frequency compressional measurements, respectively. Even in the most pessimistic case the error is far less than the signal range for each wave type observed.

3.2. Delay Times Across Iceland

[16] Delay time variations clearly show the presence of a low-velocity anomaly, circular in map view, beneath central Iceland. Stations on the event-ward side of Iceland have relatively early arrivals while stations furthest from the event are delayed (after removing delay due to epicentral distance variations). The delay at coastal stations perpendicular to the station-event azimuth drops to near-zero, indicating that the low-velocity heterogeneity is centered beneath Iceland. The RMS relative delays across the network are 4.85, 1.51, and 1.37 s for shear, low- and high-frequency compressional arrivals respectively. These estimates are larger than previously reported. *Tryggvason et al.* [1983] observed a 0.5-s relative delay for P arrivals, while *Bjarnason et al.* [1996] report 1 s for P and 3 s for S arrivals. The larger delays we observe are probably due to the wider extent of our combined networks. While the delay maps for P, *PKIKP*, S, and *SKS* all show consistent variations, we found *PP* and especially *SS* to be more variable. This is probably due to the high sensitivity of the phase to near-surface heterogeneity at the bounce point [*Hung et al.*, 2000]. We therefore decided to remove all *PP* and *SS* arrivals times from the data set.

3.3. Removing Crustal Signature

[17] Not only do the teleseismic rays travel through our target zone, the mantle, but they also pass through the crust where they are all near vertical. The parallel nature of the rays in the crust prevents resolution of crustal thickness or velocity structure, requiring many mantle tomographic studies to use station corrections [*Wolfe et al.*, 1997; *Foulger et al.*, 2000]. Station corrections are free parameters added to the inversion to absorb ray travel time anomalies associated with the region directly beneath the station. The same correction is applied to all rays arriving at the station.

[18] In this study we take a different approach. We use the 3-D crustal velocity model for Iceland, ICECRTb [*Allen et al.*, 2002], to calculate the crustal travel time for each ray and remove it from the teleseismic delay times. ICECRTb was derived primarily from Love waves, so both the crustal and mantle S velocity models are derived from *SH* waves. We remove the crustal signal by tracing the teleseismic ray

through the mantle and up through the crustal model. The travel time for the ray segment above 50 km is calculated by summing a crustal portion calculated using ICECRTb, and a mantle portion (from the ICECRTb Moho to 50 km depth) calculated using an average uppermost mantle velocity. In the case of a V_S inversion, ICECRTb provides crustal velocities and model ICAV (see section 4) provided the uppermost mantle velocity as a function of depth. For a V_P inversion the crustal velocity is obtained from ICECRTb using the linear V_P/V_S relation $V_P/V_S = 1.78 + 0.004d$, where d is the depth in kilometers [*Allen et al.*, 2002]. In the absence of a 1-D P velocity model we use a constant uppermost mantle velocity of 7.65 km/s based on the apparent velocity of first arrivals at distances of 215 to 255 km from two large earthquakes in Iceland.

[19] These corrections are made to the teleseismic travel times prior to inversion removing all crustal signal from our data vector. The data for each event are then demeaned. The mantle models are parameterized from 50 to 1000 km depth though lateral variations in the mantle velocity above 50 km are allowed as we include the ray segment from 50 km to the Moho in the mantle inversion. Through this approach we have separated the crustal and mantle signal, and as a result the remaining data vector contains only travel time deviations due to velocity anomalies below the crust.

3.4. Inversion for Mantle Structure

[20] Mantle velocity variations are parameterized on a Cartesian grid of nodes. The grid extends from a depth of 50 to 1000 km and 1000 km in both horizontal directions. The node spacing is 25 km in both the horizontal and vertical directions. The region parameterized is more expansive than the volume in which we expect to resolve structure in order to ensure that anomalies are not compressed into the model box. Rays are traced through the 1-D Earth model IASP91 and projected onto our model grid. We add an additional parameter for each event to accommodate any baseline shift between the relative travel time sets for each event. The addition of this second parameter type requires scaling of the linear system by the a priori model covariance matrix. For the velocity nodes we use standard deviations equal to 3% of the background velocity model at the appropriate depth. We effectively put no constraints on event corrections and allow them to be as large as necessary. Thus we construct a linear system for our nondimensionalized model $\mathbf{m}$:

$$\mathbf{Am} = \mathbf{d}, \tag{3}$$

where $\mathbf{A}$ is the matrix and $\mathbf{d}$ is the data vector. In addition, we impose that our model, $\mathbf{m}$, be smooth which is achieved with the smoothing matrix, $\mathbf{S}$, by setting $\mathbf{m} = \mathbf{Sy}$. $\mathbf{S}$ is a convolution filter with weights decreasing linearly in a spherical volume from zero radius to 60 km. Our new system is

$$\mathbf{ASy} \equiv \mathbf{By} = \mathbf{d}. \tag{4}$$

[21] As usual, our system of equations is inconsistent and underdetermined due to errors and the limited size of the data set. We therefore solve the system by least squares, finding the best fit model which minimizes the objective function, $\|\mathbf{By} - \mathbf{d}\|^2$. This is achieved using the LSQR algorithm [*Paige and Saunders*, 1982], which iteratively solves the system to find an approximation to the solution which has a minimum norm. While this approach prevents the introduction of components not constrained by the data, it may also introduce large individual model parameters if doing so reduces the objective function. This may include fitting noise. To compensate for this we regularize the system by introducing damping. This adds an additional set of constraints, one per model parameter, that biases the model toward zero. The objective function to be minimized becomes $\|\mathbf{By} - \mathbf{d}\|^2 + \lambda\|\mathbf{y}\|^2$ where λ is the damping factor controlling how much the model parameters are biased toward zero. The model is then reconstructed from $\mathbf{y}$, i.e., $\mathbf{m} = \mathbf{Sy}$.

[22] We experimented with a range of damping parameters (0.0 to 1.0). The final choice in the parameter is a trade-off between damping as little as possible in an effort to reduce the model residual to our measurement error (section 3.1), and preventing large-amplitude, small-volume, spikes in the velocity model which are most likely due to fitting noise in the data. Our final choice of the damping parameter was 0.2 which results in a peak S velocity anomaly of -3%. While the RMS model misfit remained above the measurement error given this choice, decreasing the damping any further resulted in significant increases in the roughness of the models. For the S velocity model, a damping parameter of 0.1 results in -4% blobs, 0.05 damping results in -5%. A greater degree of damping does not significantly change the geometry or roughness of the models but simply reduces their amplitude. For example, 0.4 damping reduces the core of the low-velocity anomaly to -2% S velocity.

4. Constraining Absolute Uppermost Mantle Velocity

[23] The primary tool we use to investigate velocity anomalies in the upper mantle beneath Iceland is teleseismic body wave tomography as discussed in section 3. Because of uncertainties in event location and origin time and delays acquired outside of the Iceland area, only delay differences between stations are significant, and no information about absolute velocity is obtained. We compensate for this using long-period surface waves to sample the absolute S velocities in the mantle beneath Iceland. This is achieved by measuring the phase of the Love wave fundamental mode at HOTSPOT stations.

[24] To obtain the phase measurement, we fit the full waveform in a time window associated with group velocities between 3.45 and 4.6 km/s. The use of this group velocity window allows us to select the fundamental and higher modes sampling the upper mantle while cutting out data associated with body waves sampling the lower mantle. This is achieved by minimizing the misfit between the data and a synthetic waveform calculated by mode summation using the earthquake source parameters (we use the Harvard centroid moment tensor (CMT) solution) and a 1-D Earth model [*Nolet*, 1990]. This approach not only prevents contamination of the measurement by higher modes (as we account for them in the fit) but also constrains the phase measurements to a smooth phase velocity curve which is a functional of a realistic layered Earth model.

[25] The 10 events used (Figure 3a) are at epicentral distances of 7 to 73° and give good azimuthal coverage.

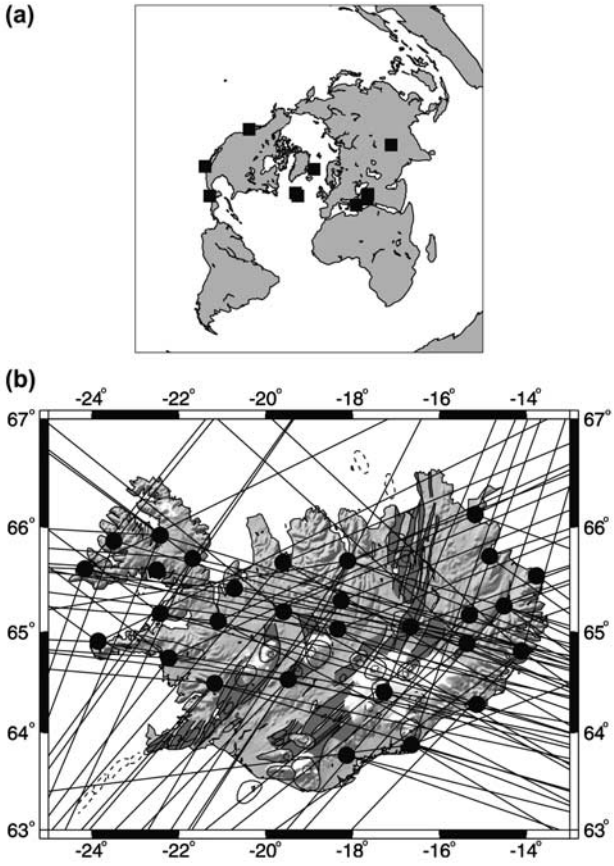

Figure 3. Map of (a) events and (b) stations and paths used in surface wave study. The stations (circles) are from the HOTSPOT network, the 10 events used (squares) represent good azimuthal coverage resulting in paths crossing sufficiently to measure both average phase velocity and perturbations across Iceland.

The source-receiver paths associated with the 139 phase measurements are shown in Figure 3. Since good waveform fits are not obtained for data contaminated with multiple arrivals, such cases are easily identified and the waveforms rejected. In order to sample as the upper mantle we fit waveforms in the frequency range 0.015 to 0.04 Hz corresponding to wavelengths in the 100 to 300 km range. The aperture of the HOTSPOT network is 500 km east–west and 300 km north–south, and the average station spacing is about 50 km. Changes in the wave number are therefore being measured over distances less than the typical wavelengths (100–300 km). For this reason we must be wary of small variations in the phase as a function of frequency that could significantly contaminate our measurements. The use of a smooth phase velocity curve derived from the synthetic waveform fit prevents such contamination.

[26] We use the phase measurements as constraints on variations in the wave number beneath Iceland. The linear system we solve is

$$\phi_i(f) = E_c + k_{avg}(f)\Delta_i + \sum_j A_{ij}\delta k_j(f), \qquad (5)$$

where ϕ_i is the phase for path i, E_c is the event correction, a constant for each event, k_{avg} is the average wave number over all events at frequency f, Δ_i is the epicentral distance, **A** is a matrix of path lengths associated with each node, and δk_j is the wave number perturbation for each node j. We invert the above system for each of the discrete frequencies for which we have phase measurements obtaining an average wave number and variations in the wave number on a horizontal grid of nodes, spacing 1°. We choose two frequencies with which to proceed based on the number of phase measurements available and the consistency of the measurements. At 0.0195 Hz the initial RMS of the phase measurements is 0.254 rad, the final RMS is 0.186 rad corresponding to a variance reduction of 46%; the average phase velocity is 4.20 km/s. At 0.0244 Hz the RMS is reduced from 0.315 to 0.210 rad, a 55% variance reduction, and the average phase velocity is 4.17 km/s.

[27] Finally, we invert our average phase velocities for an average 1-D *S* velocity model beneath Iceland. The starting model is derived from IASP91 [*Kennett and Engdahl*, 1991], replacing the upper 30 km with an average crustal model for Iceland [*Allen et al.*, 2002]. We fix the crustal velocities and solve for sub-Moho V_S. Below 120 km depth we require a smooth transition back to the starting model at 210 km depth. We experimented with the depth extent of the basis functions in the inversion. If they extended only to shallow depths (say 100 km), the phase velocity observations could only be satisfied by a model with very low velocities immediately beneath the crust (i.e., less than the lower crustal velocity). Our preferred model departs from IASP91 above 210 km as shown by the long dashed line in Figure 4. The *S* velocity gradient from 210 km depth to the Moho can be approximated as $V_S = 3.97 + 0.0026d$, where d is the depth in km. We refer to this model as ICAV. Extrapolated, this gives reasonable estimates of the average *S* velocity just below the crust: 4.0 km/s when the Moho is at 15 km and 4.1 km/s at 46 km, depths corresponding to the thinnest and thickest crust on Iceland. This compares to lowermost crustal velocities of 3.8 km/s and *Sn* velocities of 3.9 to 4.4 km/s [*Allen et al.*, 2002].

5. Mantle Structure

[28] The three linear systems constraining *S* velocity structure as sampled at 0.03–0.1 Hz, and *P* velocity structure sampled at 0.03–0.1 and 0.8–2.0 Hz, are inverted separately for mantle velocity structure. The result is three independent velocity models for Iceland.

5.1. *S* Velocity Structure

[29] The *S* velocity model is generated using data from 136 teleseismic events recorded at the 78 stations. There are 1814 rays; 1650 are direct *S* phases, the remaining 164 are *SKS*. The ray density distribution is shown in Figure 5. The initial RMS misfit is 1.38 s. After inversion the RMS is reduced to 0.50 s, which is still higher than our estimate of the measurement error from cross correlation which was 0.05 to 0.25 sec. Although we tried reducing the damping factor to reduce the RMS further, this led to a significant increase in roughness of the model. The discrepancy between the measurement error and feasible RMS reduction suggests that the inadequacies of our theoretical approach, i.e., the assumption of ray theory, and Fermat's principle,

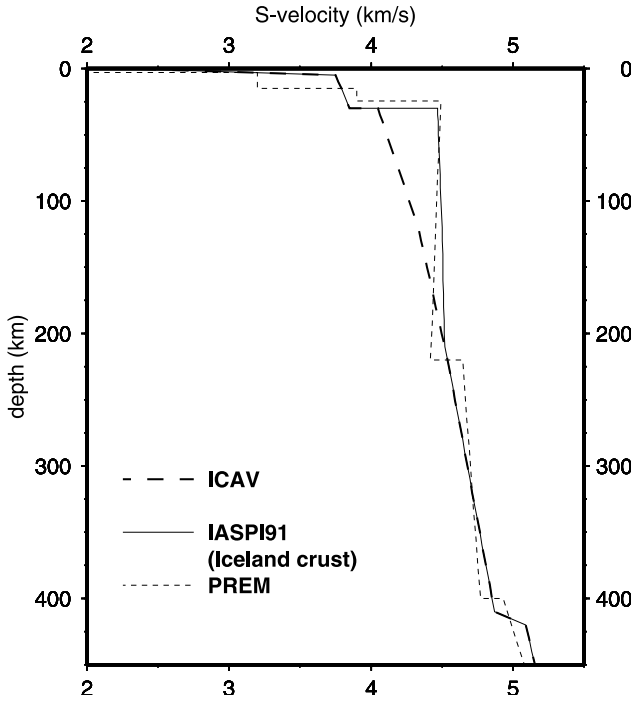

Figure 4. The 1-D average mantle *S* velocity model for Iceland: ICAV (dashed line). The model was derived from average phase velocity measurements across Iceland which were used to invert for mantle velocity in the upper 210 km. Also shown are the Earth models IASP91 (with the average velocity model for the Iceland crust inserted) (solid line), and PREM (short dashed line), both of which have near constant velocities of ~4.5 km/s in the upper 200 km of mantle.

along with the assumption of isotropy, are perhaps more significant than the errors in our measurement.

[30] The *S* velocity model is the only one for which we have knowledge of the absolute velocities in the upper mantle. The absolute velocity information comes from ICAV (Figure 4) which we combine with the lateral velocity variations obtained from body wave tomography. The result is shown in Figures 6a and 6b, which are vertical slices through the *S* velocity model ICEMAN-S across, and parallel, to the rift axes on Iceland (see lines on inset maps). As we have no absolute velocity information below 210 km, we simply plot the lateral variations; above 210 km we plot the percentage deviation from 4.5 km/s. We choose 4.5 km/s because both Earth models IASP91 and PREM [*Dziewonski and Anderson*, 1981] have near-constant velocities of 4.5 km/s from ~200 km up to the base of the lithosphere (see Figure 4). We are therefore plotting percentage velocity anomalies from these Earth models.

[31] The result is a cylindrical low-velocity anomaly extending from at least 400 km depth up toward the surface where it spreads out beneath the lithosphere: consistent with a plume conduit feeding an extensive plume head as envisioned in the original plume model [*Morgan*, 1971]. Previous studies of the Icelandic mantle have been unable to image the plume head since it is a predominantly horizontal structure and therefore generates only small differences in relative teleseismic travel times. At depth, the maximum low velocity in the core of the plume is −3.5%; just beneath the base of the lithosphere the anomaly is up to −10%, a velocity of 4.05 km/s. Within the plume head, above the plume core, there is an anomalous region where the velocity remains constant from ~70 to ~150 km depth.

[32] To emphasize other aspects of the velocity structure, we also plot just the lateral velocity variations for the same slices in Figures 6c and 6d. With the plume head removed, we see variations within it more clearly. At depth, the structure remains the same. Around 200 km depth, the low-velocity anomaly begins to reduce in lateral extent and come to a point above the plume core, below central Iceland. There is a low-amplitude low-velocity anomaly which extends off to the side of the main anomaly in Figure 6c and reaches the surface beneath the Snæfellsnes Peninsula (Figure 1). In Figure 6 the upper 50 km is blocked out gray as the top of our model box is at 50 km. Above the plume core, from ~100 km to the base of the Moho, there is a relatively high velocity, up to +2%, a feature absent in previous images. It is only detectable in our model because we are able to remove the crustal signature from the travel time data. As the rays are near vertical, particularly in the upper part of the model, vertical resolution is problematic and velocity variations are vertically smeared resulting in the possibility of high and low anomalies cancelling each other out. The crustal model ICECRTb contains a low-velocity zone extending through the entirety of the crust in central Iceland directly above this high velocity. Without the removal of the crustal signature from the mantle data set these two anomalies smear together preventing imaging of the uppermost mantle high velocity.

5.2. *P* Velocity Structure

[33] The low-frequency *P* velocity model uses 2103 rays from 148 teleseismic events, of which 1893 rays are *P* and 210 are *PKIKP*. The initial RMS misfit of 0.41 s is reduced to 0.24 s compared to the data error estimate of 0.04–0.20 s. We name this velocity model ICEMAN-LP. The high-frequency *P* velocity model is the only one to use data from the short-period SIL stations (Figure 1). As a result, it is derived from the largest number of rays, 2695 including 2595 *P* arrivals and 100 *PKIKP*, generated by 146 events. The estimated data error was 0.02–0.10 s which we did not attempt to reach for the same reason as with the *S* model. The initial RMS was 0.34 s, the final, 0.17 s. We name this model ICEMAN-HP. The ray density distributions for both models are shown in Figure 5. Given the two independently derived *P* velocity models, we can test the extent to which one model satisfies the other travel time data set. Given the ICEMAN-HP solution, the low-frequency travel time RMS is reduced from 0.41 to 0.35 s. Given the ICEMAN-LP solution, the high-frequency travel time RMS is reduced from 0.34 s to 0.30 s.

[34] The lateral velocity variations are shown in Figure 7. All three velocity models are shown for comparison: two vertical slices, one parallel, one across the rift, and four horizontal slices at depths of 75, 200, 300, and 400 km.

5.3. Comparison of *P* and *S* Velocity Structure

[35] At 300 to 400 km depth, there is a single low-velocity anomaly beneath central Iceland (Figure 7) with a maximum V_S anomaly of −3.5% and maximum V_P anoma-

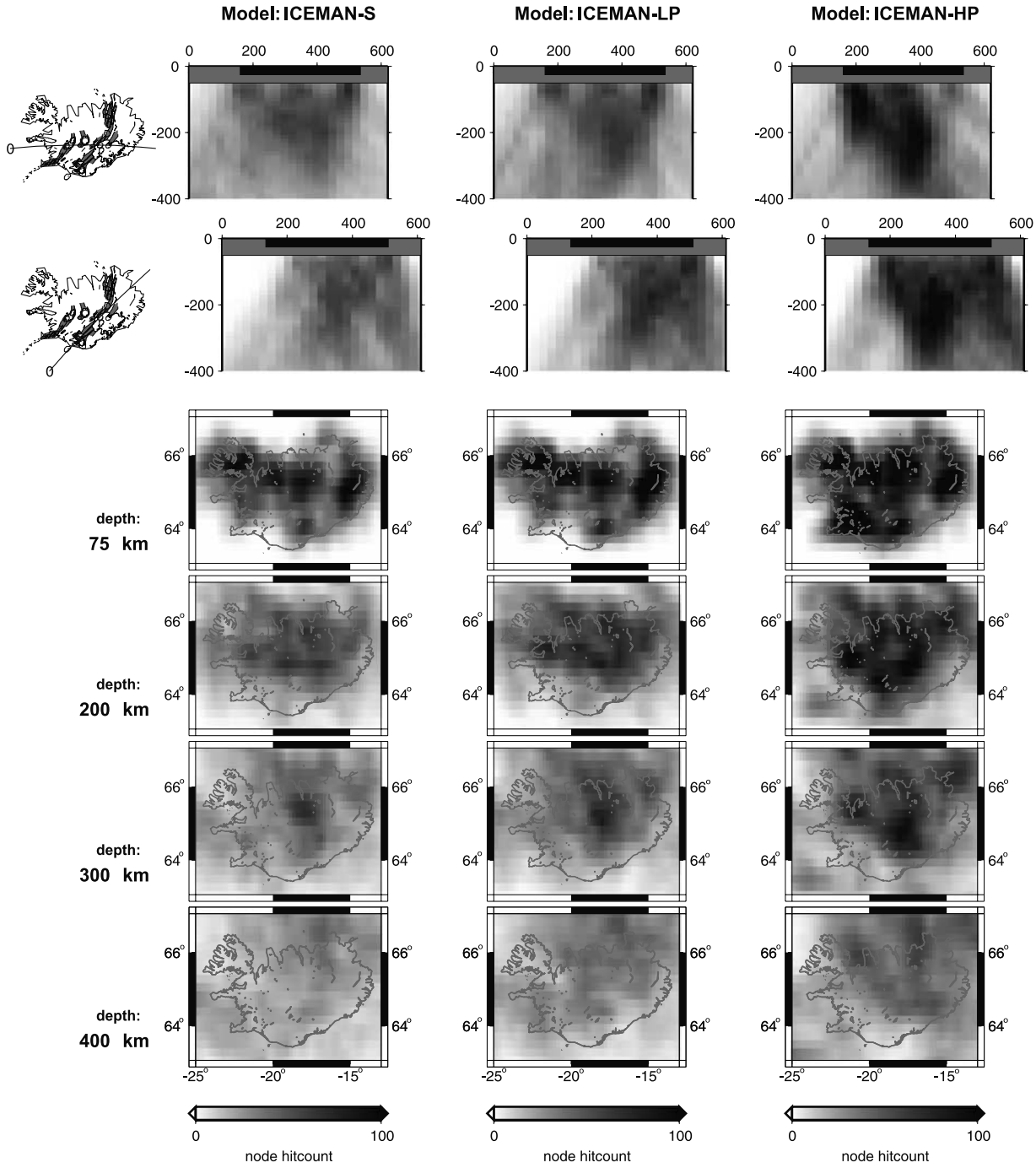

Figure 5. Ray density (hit count) plots for models ICEMAN-S, ICEMAN-LP, and ICEMAN-HP. The number of rays contributing to the velocity determination of each node for each velocity model is counted. This hit count is plotted for the same slices as the velocity models (Figures 6 and 7): vertical slices across and parallel to the rift (location shown by the line on the adjacent maps, black bars on slices indicate the location of Iceland), and horizontally slices at depths of 75, 200, 300, and 400 km as indicated to the left. Note that ray density alone is not a good indicator of model resolution, Figure 8 shows the results of resolution tests.

lies of −2.0% and −1.75% in ICEMAN-LP and ICEMAN-HP, respectively. The anomaly is characterized as pseudo-cylindrical, it is ∼200 km wide east–west and appears to be elongated north–south in some of the model slices. Any elongation is most apparent in ICEMAN-HP at both 300 and 400 km depth where the anomaly is ∼400 km north–south; however, there is little evidence of elongation in ICEMAN-LP. ICEMAN-S suggests elongation at 400 km, but the anomaly is more circular at 300 km. We tested if such an elongation is resolvable in our model using a synthetic velocity model with a vertical, cylindrical low-velocity anomaly, Gaussian in cross section and extending

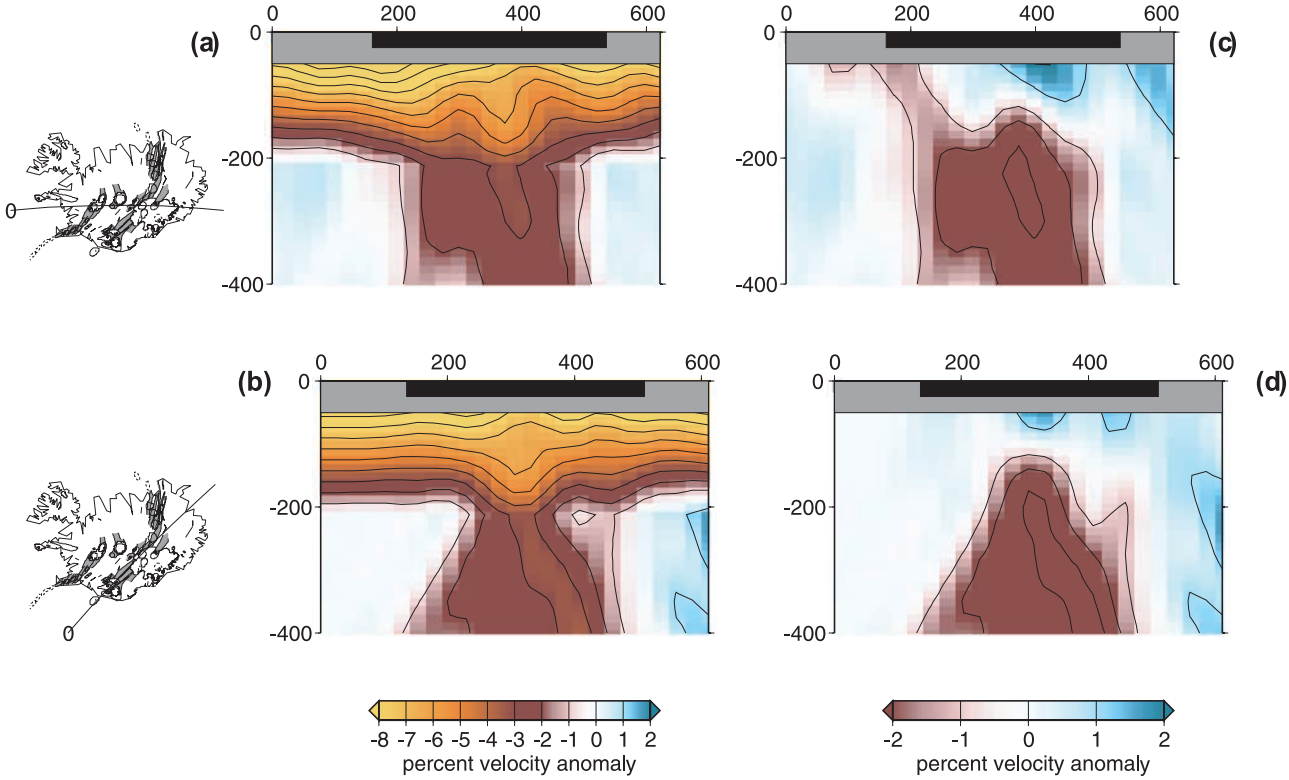

Figure 6. Vertical cross sections through the mantle *S* velocity model ICEMAN-S. (a) and (b) Absolute velocity variations obtained by combining the absolute average velocity (ICAV) with variations for sections across (Figure 6a) and parallel (Figure 6b) to the rift on Iceland. The slices show percentage deviation from 4.5 km/s in the upper 210 km where absolute velocity is constrained, and the percentage deviation from the layer average below 210 km. The slices illustrate both the vertical plume conduit at 400 to ~200 km depth and the horizontal plume head above 200 km. (c) and (d) Relative velocity anomalies across (Figure 6c) and parallel (Figure 6d) to the rift enable visualization of the velocity variations within the plume head including high velocities in the uppermost mantle above the plume core. The location of the slices is show by the lines on the adjacent maps. The black bars on the slices indicate the location of Iceland.

through the model box beneath central Iceland (first resolution test, Figure 8). After generating synthetic data and inverting (we do not add noise), we recover the cylindrical anomaly very well with no north–south smearing which suggests any elongation in our models are not an artifact of ray geometry. *Foulger et al.* [2000] observe a more extensive north–south elongation in their model at 300–400 km depth which they suggest indicates that the base of the plume conduit is located in the upper mantle. Here we are wary of such an interpretation as this elongation is not consistently observed in all of our models despite resolution more than adequate to detect it. In the 300–400 km depth range the *S* velocity anomaly is typically twice the *P* anomaly which we expect based on our observation that the *S* delays across Iceland are ~4 times the *P* delays.

[36] Above ~250 km the overall velocity structure changes radically in all three models, and the single low-velocity anomaly at depth is replaced by more complex structure. The 200-km depth slices cut through narrow extensions of the deep, low-velocity anomalies which reach shallower depths (see vertical slices in Figure 7). Whereas the *S* velocity anomaly is twice the *P* anomaly at depth, above 200 km this is not the case. At 200 km the *S* anomaly reaches −3%, and the *P* anomaly reaches only a third of that, −1%. Above ~100 km all three models show high-velocity anomalies above the plume core beneath central Iceland. The maximum anomalies are +2%, +2%, and +1.5% for ICEMAN-S, ICEMAN-LP, and ICEMAN-HP, respectively. This change of structure above and below 200–250 km is well within resolution. If the low-velocity structure imaged at depth were to extend up to the surface, it would be easily recovered as demonstrated by the first resolution test shown in Figure 8.

[37] In the second set of resolution tests shown in Figure 8, we input a high-velocity anomaly between 50 and 150 km and a low-velocity anomaly vertically beneath at 300 to 400 km depth. Both anomalies have a Gaussian radius of 50 km. Again the synthetic anomalies are recovered very well with minimal vertical smearing. We conducted many more resolution tests in an effort to understand the velocity structures we expect to resolve. In the lower, plume conduit portion of the model we could resolve 50 km radius, 100-km-high blobs of low-velocity material if they were vertically separated by more than 100 km. In the upper 200 km of the model we are able to recover 25 km radius spheres with some vertical smearing. These tests demonstrate that

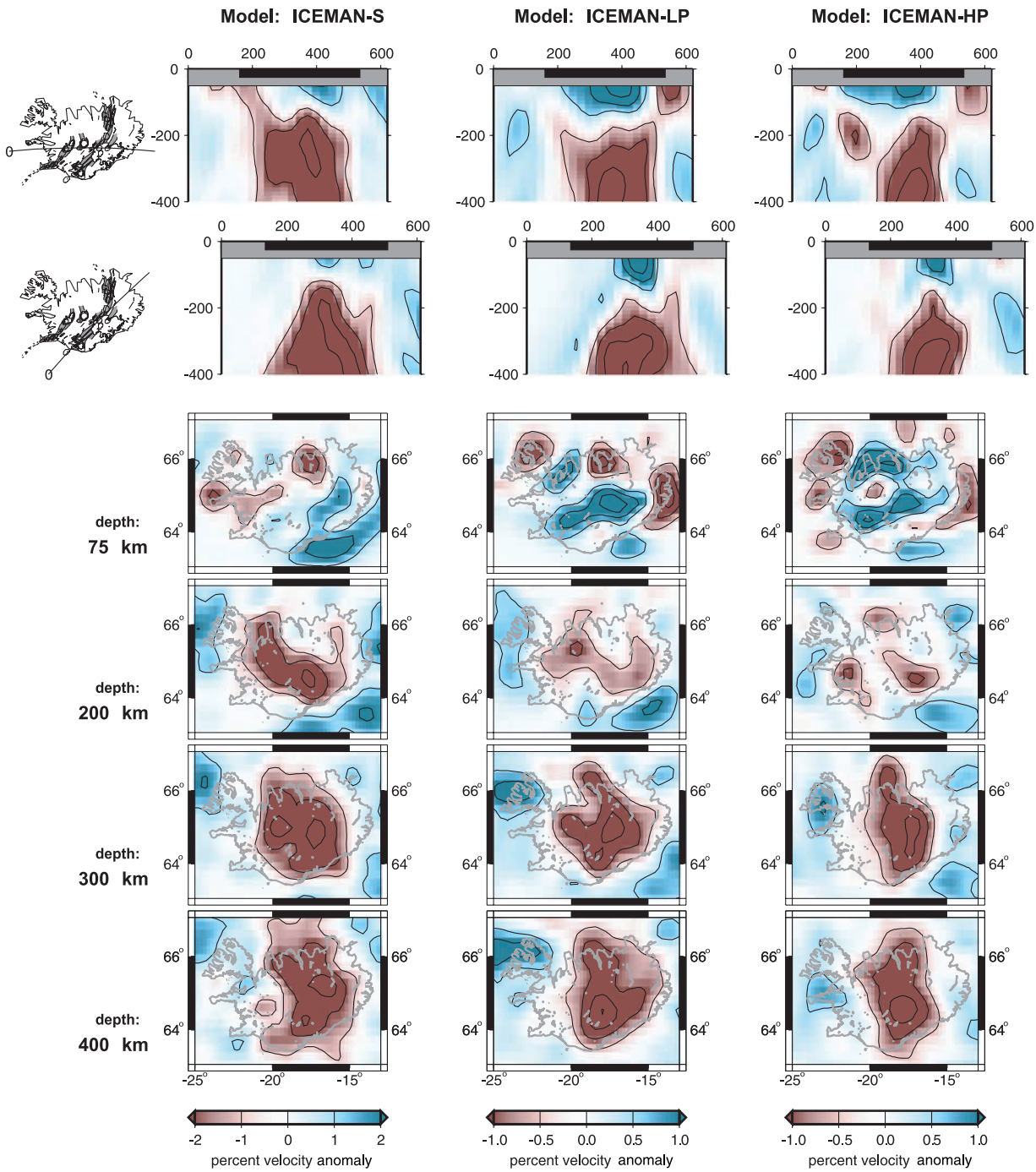

Figure 7. Relative velocity anomalies for models ICEMAN-S (*S* velocity derived from 0.03–0.1 Hz travel time observations), ICEMAN-LP (*P* velocity derived from 0.03–0.1 Hz observations), and ICEMAN-HP (*P* velocity derived from 0.8–2.0 Hz observations). Each model is sliced across and parallel to the rift (locations shown by lines on adjacent maps, black bars on the slices indicate the location of Iceland) and horizontally at depths of 75, 200, 300, and 400 km as indicated to the left. The main features of the velocity structure beneath Iceland are (1) a low-velocity cylindrical anomaly extending from 400 km up to 200 km depth; (2) a significant change in the nature of the anomalies above 200–250 km due to the presence of a horizontal plume head (see Figure 6); and (3) a high-velocity anomaly in the uppermost mantle above the plume core beneath central Iceland.

our resolving power is significantly better than the scale of features discussed.

[38] The third resolution test shown in Figure 8 is designed to test the maximum detectable diameter of the low-velocity anomaly beneath Iceland. The synthetic model consists of a broad vertical cylinder with a Gaussian cross section of radius 500 km. Our ray set is unable to recover the full diameter of the anomaly as it is considerably wider

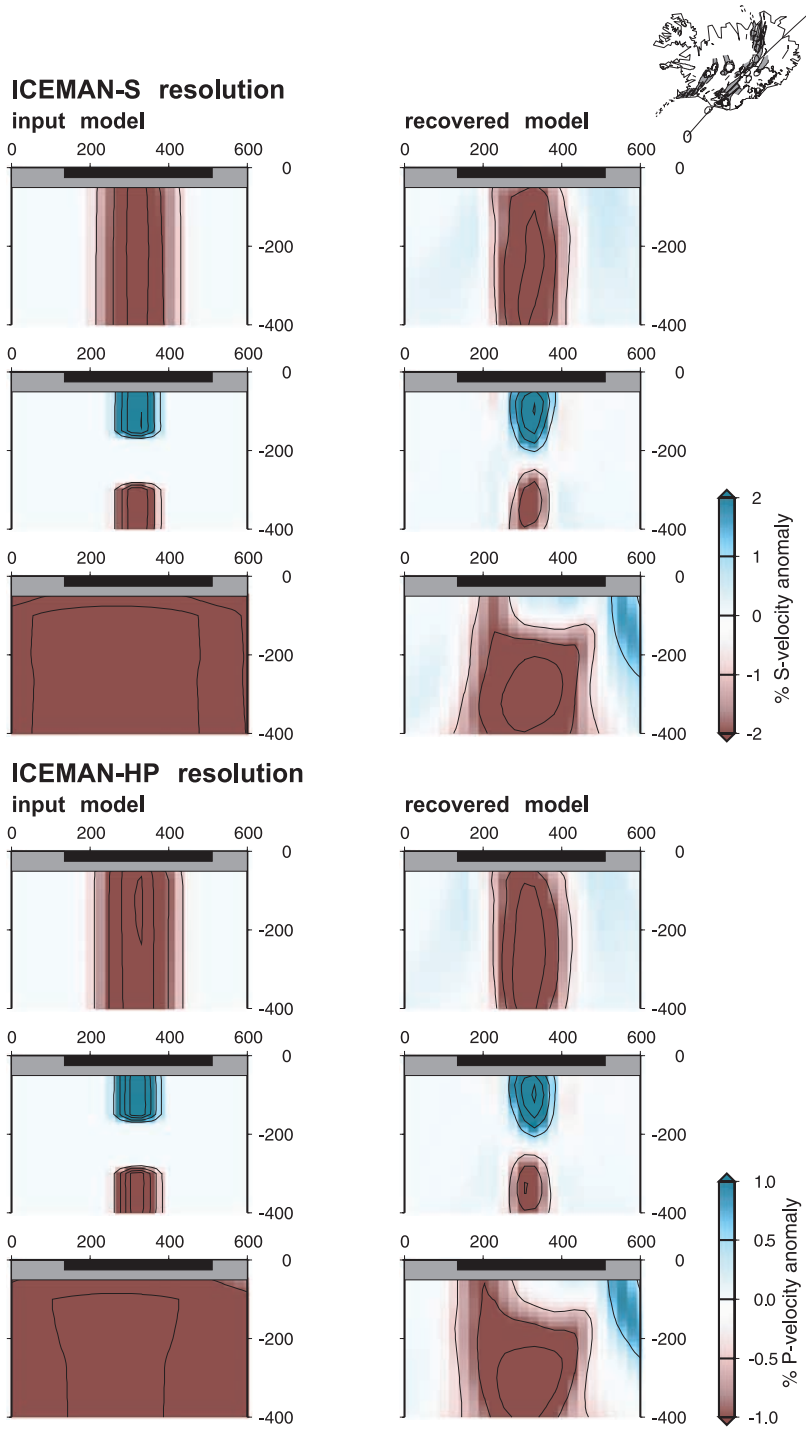

Figure 8. Resolution tests using ray sets available for ICEMAN-S and ICEMAN-HP. For each model we show the results of three tests. Vertical slices through the input synthetic anomaly are shown to the left, and the recovered anomaly is to the right. The first test demonstrates that if the low-velocity anomaly observed at depth extended up to the surface, it would be easily recovered. The second test illustrates the vertical resolving power of the ray sets. The high- and low-velocity anomalies are not smeared together. The third test shows the maximum diameter anomaly that the ray sets are able to resolve. The input anomaly is broader than Iceland and the ray sets, and only the central portion is recovered; however, the resolved region is broader than the anomalies observed (Figure 7).

than the seismic network. The recovered anomaly is narrower, the best fit Gaussian-shaped anomaly has a radius of ~180 km for both the *P* and *S* velocity models. This represents the maximum diameter anomaly that our data set can recover, which is 2 to 3 times broader than the observed anomalies. The Gaussian-shaped anomalies which best fit our observed velocity models have radii of 60–80 km for ICEMAN-HP, 60–100 km for ICEMAN-LP, and

60–100 km for ICEMAN-S. The recovered velocity structure is also near zero in the upper ~100 km. This is due to the insensitivity of relative teleseismic travel time data to a horizontal velocity anomaly close to the surface and extending beneath all the stations and is why we have included surface wave constraints in our models.

6. Discussion

6.1. Interpretation of Plume Conduit Velocity Anomalies

[39] In the plume conduit (200–400 km depth) the core anomalies are −3% for *S* velocity and −1.5% for *P* velocity. Before attempting to interpret these velocities we note that they are almost certainly minimum estimates for several reasons. The inversion scheme used imposes smoothing and damping of the velocity model. We can estimate this effect with resolution tests. Figure 8 shows the results of a test where we input a velocity anomaly of similar amplitude and geometry as the plume conduit at depth. We recover about 80% of the anomaly for ICEMAN-S and 70% for ICEMAN-HP. This would imply the real Earth velocity anomalies in the plume conduit could reach −3.8% and −2.1% for *S* and *P* velocity, respectively. These values are similar to those previously obtained in tomographic models for Iceland [*Wolfe et al.*, 1997; *Foulger et al.*, 2000] and are easily interpreted in terms of an excess temperature anomaly consistent with the geochemical estimates of 140–260°C [*McKenzie*, 1984; *Schilling*, 1991; *White et al.*, 1995; *Shen et al.*, 2002].

[40] We do not attempt to estimate temperature from the tomographically inferred wave speed due uncertainties in tomographic estimates. Instead, we take geochemical estimates of the plume temperature anomaly and using laboratory measurements of temperature derivatives we calculate the expected velocity anomalies. The results are shown in Table 2. When attenuation, Q, is considered, the velocity estimates are in the range of those observed. For example, if ∂T = 250 K and Q_S = 100, we calculate an *S* velocity anomaly of −3.8%, consistent with our observations. The simple relation $Q_P = 9Q_S/4$ suggests the corresponding value of Q_P is 225. The closest tabulated value is for Q_P = 200 (Table 2) which would predict a *P* velocity anomaly of −2.5%. For a Q of 225 the velocity anomaly would be a little lower, in line with the observed −2.1%.

[41] Another, and perhaps more significant reason that our velocity anomaly estimates in Figure 7 are a minimum, is that ray theory does not account for wave front healing effects which cause a loss of travel time signal [*Wielandt*, 1987]. Although our stations are close to the anomaly and ICEMAN-HP uses high frequencies which reduce this effect [*Nolet and Dahlen*, 2000], the decay of the travel time delay is significant. *Allen et al.* [1999] use a 2-D finite difference code to investigate the diffraction effects of a cylindrical plume on the frequency-dependent amplitudes of shear arrivals as measured above the plume. Through comparison of forward calculated variations with observations on Iceland they concluded that the *S* velocity anomaly has a radius of 100 km and a maximum velocity anomaly as large as −12%. The ray theoretical travel time delay for such an anomaly would be 7 s; however, when wave front healing is accounted for, the delay drops to 4 s, within the range we observe. We are therefore forced to conclude that it is possible that the velocity anomalies are much greater than shown in Figure 7, which has significant implications for the temperature, composition and partial melt properties within the plume core at depth.

Table 2. Comparison of Velocity Anomalies Expected for Temperatures in the Range of Geochemical Estimates for Iceland[a]

Q	$\partial \ln V_P/\partial T$, $\times 10^{-4}$ K^{-1}	$\partial \ln V_S/\partial T$, $\times 10^{-4}$ K^{-1}	V_P, % ΔT = 140 to 260 K	V_S, % ΔT = 140 to 260 K
∞[b]	−0.62	−0.76	−0.8 to −1.6	−1.1 to −1.8
200[c]	−1.01	−1.15	−1.4 to −2.6	−1.6 to −3.0
100[c]	−1.40	−1.54	−2.0 to −3.6	−2.2 to −4.0
50[c]	−2.18	−2.32	−3.1 to −5.7	−3.2 to −6.0

[a]Calculated from laboratory measurements of temperature derivatives.
[b]From *Isaak* [1992].
[c]From *Karato* [1993].

6.2. Interpretation of Plume Head Velocity Anomalies

[42] The character of the velocity anomalies in the upper 200–250 km of the mantle is clearly different to that in the deeper mantle (Figure 7). We interpret this as being due to the presence of a horizontal plume head, the bulk of which is undetectable using body wave tomography, but is visible when absolute velocities are measured (Figure 6). Recent studies of Hawaii suggest that the relatively high velocity, 90-km-thick lithosphere is underlain by a ~100-km-thick layer of low-velocity asthenosphere with velocities in the range 4.0 to 4.2 km/s [*Priestley and Tilmann*, 1999; *Nataf*, 2000, Figure 9]. These velocities are similar to those in the uppermost mantle beneath Iceland. While such velocities are ~5% less than for normal 80–90 Ma oceanic mantle (the age of the crust beneath Hawaii), they are expected for zero age mantle [*Nishimura and Forsyth*, 1989]. The uppermost mantle velocities in ICAV, however, represent an average for the 0–20 Ma Icelandic lithosphere. The observed average of 4.1 km/s beneath Iceland is therefore still lower than expected.

[43] Perhaps the most surprising aspect of our mantle velocity model is the relatively high velocities in the uppermost mantle above the plume core. This feature is clearly visible in all three models with a core V_S anomaly of 2% and V_P of 1.5–2% (Figure 7). Similar anomalies are absent in all previous studies of the mantle beneath Iceland. To test this observation, we use our teleseismic surface wave measurements. As described in section 4, we inverted the phase measurements not only for an average phase velocity, from which ICAV is derived, but also construct a map with deviations from this average on a 1° grid. We use these variations in phase velocity to derive 1-D *S* velocity models for the mantle beneath each of our well resolved grid points, a total of 11 models across Iceland. The approach is the same as for ICAV: the average crustal model beneath each grid point is obtained from ICECRTb, it remains fixed, and we vary the mantle velocity to a depth of 210 km in order to satisfy the phase velocity. Although the scatter in the surface wave phase velocities is larger, the clear trend in these 1-D velocity models provide an independent estimate of velocity variations across Iceland. Figure 9 is a comparison of the horizontal velocity variations resolved with our body wave and surface wave observations at depths of 50 and 100 km.

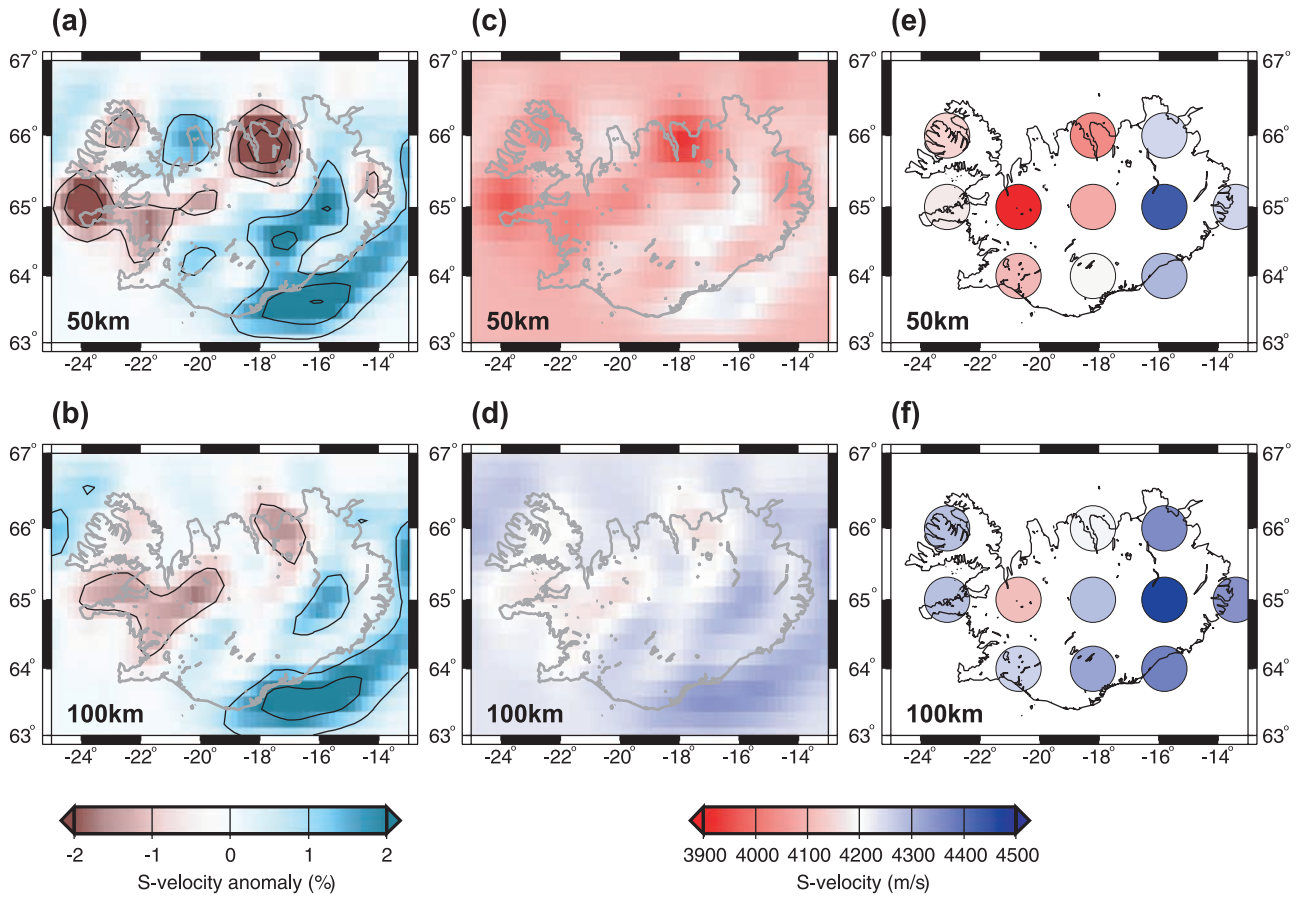

Figure 9. Comparison of velocity anomalies at 50 and 100 km depth derived independently from body wave tomography and surface wave phase velocity measurements. First, we show horizontal slices through our *S* velocity model ICEMAN-S at (a) 50 and (b) 100 km depth. Using the average absolute velocity from ICAV, we convert the percentage variations shown in Figures 9a and 9b to absolute velocity shown in Figures 9c and 9d. Thus the velocity variations in Figures 9c and 9d are derived from the body wave tomography. Figures 9e and 9f show absolute velocity variations derived from phase velocity variations across Iceland. The surface wave observations (Figures 9e and 9f) not only support the body wave observations that there are relatively high velocities below central Iceland, but they also suggest that they are even higher.

Figures 9a and 9b show the percentage *S* velocity anomaly from ICEMAN-S as shown in Figure 7. In Figures 9c and 9d we use our average velocity model ICAV to relate these percentage variations to absolute velocity. Figures 9e and 9f are the absolute velocity estimates from the surface wave phase observations plotted with the same scale as Figures 9c and 9d. These independent observations show good agreement. They show relatively high velocities beneath eastern Iceland, low velocities extend along the Snæfellsnes Peninsula, continue inland, and are also found beneath the central north coast. In fact, the surface wave data not only support the high-velocity observations from body wave tomography but suggest even higher velocities.

[44] As we use the Icelandic crustal model ICECRTb both to correct the teleseismic travel time delays for the body wave tomography and in our inversion of phase velocities across Iceland, we must ensure that any errors in ICECRTb are not responsible for the mantle high-velocity anomaly. For example, an erroneously thick crust would require compensation in our mantle velocity models, high velocities directly beneath the thick crust would achieve this. Also, crustal velocities that are too low could cause velocities too high elsewhere. However, the low amplitude and small volumes of ICECRTb velocity anomalies make the size of any associated vertical travel time delays small compared to those due to movements of the Moho. We therefore consider the effect of errors in crustal thickness. We achieve this by determining the vertical distance the Moho would be required to move to remove the uppermost mantle high velocities. The vertical travel time delay through the center of the uppermost mantle high-velocity anomaly in ICEMAN-S is −0.25 s. To estimate the vertical travel time delay resulting from moving the Moho, we use a velocity step across the Moho of 3.7 to 4.1 based on the average properties of the Moho from surface wave studies [*Allen et al.*, 2002]. Moving the Moho up by 1 km results in a travel time delay of −0.026 s. Note, however, that in central Iceland the lower crustal velocities are lower than average; hence the real delay resulting from moving the Moho 1 km will be less than −0.026 s. It follows that crustal thickness must be reduced by more than 10 km to remove the uppermost mantle high velocity from ICEMAN-S. Performing the same calculation for the *P* velocity models has a greater uncertainty as we do not have good estimates of

uppermost mantle P velocity. Refraction studies of central Iceland suggest a lowermost crustal velocity of 7.35 km/s [*Staples et al.*, 1997; *Darbyshire et al.*, 1998]. The uppermost mantle velocity is probably in the range 7.65 to 8.0 km/s. The vertical travel time delays through ICEMAN-HP and ICEMAN-LP are −0.082 and −0.117 s respectively, requiring the Moho to move 11 to 22 km for ICEMAN-HP and 8 to 15 km for ICEMAN-LP depending on the uppermost mantle velocity. The crustal thickness errors in ICECRTb are significantly smaller than the >10 km that would be required to remove the uppermost mantle high-velocity anomalies. The ICECRTb crustal thicknesses are also in good agreement with those of *Darbyshire et al.* [1998, 2000a, 2000b]. For example, the thickest crust along the ICEMELT refraction line [*Darbyshire et al.*, 1998] across central Iceland is ∼42 km (40 km Moho depth plus elevation). ICECRTb crustal thickness in the same location is 44 km.

[45] Since we are confident that these high velocities are real, their explanation is perplexing. The high temperatures and partial melt we may expect in the plume core at these depths would both result in low velocities. The mechanism of melt extraction, however, does lead to higher velocities in the residual. *Jordan* [1979] estimates that the removal of 10% basaltic melt from peridotite would cause a 1% increase in V_P; the increase in V_S would be more substantial. The result is higher-velocity residual, which becomes lithosphere, after melting. We would therefore expect high velocities in the lithosphere beneath all of Iceland and low velocities in the plume conduit melt zone beneath central Iceland due to higher temperatures and partial melt, the reverse of what we observe. Curiously, similar observations of high velocities are also found beneath some volcanoes at crustal depths (A. Rubin, personal communication, 2000). The only possible explanation of our observations is that the degree of melt currently being extracted from the plume core is higher than before, and this effect is more substantial than the velocity-lowering effect of partial melt in the current melt zone.

[46] Melt extraction models and experiments suggest that melt is removed rapidly on formation in the mantle; the threshold for removal may be as low as a few tenths of a percent [*Riley and Kohlstedt*, 1991; *McKenzie*, 2000]. Geophysical observations in Iceland also suggest only small melt fractions in the mantle. *Darbyshire et al.* [2000a] and *Staples et al.* [1997] both put an upper bound of 1% on melt fraction below the Moho based on velocity and density anomalies, respectively. In addition, laboratory experiments demonstrate that the effect of partial melt on anharmonic velocity does not become significant until the fraction of melt exceeds 2% [*Sato et al.*, 1988]. When attenuation effects are taken into account, the effect of low degrees of melt on velocity is more significant. If the low fractions of melt occupy isolated regions, however, the effect on the average velocities may be small. With these arguments we hope to have demonstrated that melt generation in the plume beneath Iceland may have only a small effect on seismic velocity.

[47] The plume is also currently in its most active state for the last ∼20 Myr as suggested by two observations. First, the crust on Iceland is equivalent to the melt thickness generated in the mantle and the thickest crust is above the current plume core [*Allen et al.*, 2002]. Second, residual height anomalies along plate flow lines in the North Atlantic have been increasing over the last 10–15 Myr [*White*, 1997], again suggesting an increase in mantle temperature over this time period.

[48] Rare earth element (REE) inversions of the basalt compositions from current rift zones on Iceland [*White et al.*, 1995; *White and McKenzie*, 1995] suggest 20–30% melting of mantle material which could cause a substantial 2–3% increase in the P velocity of the residual once the melt has been removed. While it is not clear that the increase in melt production over the last 20 Myr is associated with an increase in percentage melt, it at least provides a feasible explanation for the existence of relatively high velocities in the uppermost mantle above the plume core today.

6.3. Volumetric Flow and Eruption Rate

[49] *Sleep* [1990] estimated the volumetric flow, J_p, of the Icelandic plume by assuming it provides material for the lithosphere and an asthenospheric layer below. Assuming the top of the asthenospheric layer is traveling at the plate velocity, the bottom has zero velocity, and a linear relation between, he obtains the following relation:

$$J_p = V_f(L + A/2)Y, \tag{6}$$

where V_f is the full spreading rate, L is the lithospheric thickness, A is the asthenospheric thickness, and Y is the along-axis distance supplied by the plume. Given our image of plume structure we would change little in his estimation. We use lithospheric and asthenospheric thicknesses of 100 km and 150 km respectively and a full plate spreading rate of 18 mm/yr [*DeMets et al.*, 1994]. The along-axis estimate is the greatest uncertainty in this calculation. The length of the rift across the bathymetric swell associated with Iceland is ∼700 km, but the plume's influence is broader. Crustal thickness along the Mid-Atlantic Ridge south of Iceland does not return to its normal ∼7 km thickness until distances greater than 1000 km from central Iceland [*Navin et al.*, 1998]. Some of the geochemical signatures extend over similar distances such as $^{87}Sr/^{86}Sr$ [*Ito et al.*, 1996]. Using 800 km for the along-axis distance (the same as Sleep), and the above values, we obtain an estimated plume volume flux of 2.5 km^3/yr, a little more than Sleep's estimate of 2.0 km^3/yr.

[50] It is instructive to compare this flux to the crustal generation rate. To do this we must determine the extent of the rift axis fed by melt from the plume. The average crustal thickness on Iceland where the rift length is ∼400 km is 29 km [*Allen et al.*, 2002]. Recent seismic studies along the Reykjanes Ridge [*Weir et al.*, 2001] show the crustal thickness dropping from 16 to 12 km in the 200 to 400 km distance range from the plume center. If we assume that melt from the plume feeds 800 km of crustal formation (the same length of asthenosphere fed by the plume), then the average crustal thickness is ∼22 km, and we obtain a crustal volume flux of 0.3 km^3/yr. This estimate is probably too large, however, as melt is unlikely to travel such large distances. For a better estimate we assume that the plume melt only feeds crustal formation on Iceland. Images of both normal Mid-Atlantic Ridge [*Magde et al.*, 2000] and the

Icelandic crust [*Allen et al.*, 2002] suggest that magma is piped vertically through the lower crust and then spreads horizontally along the ridge axis at upper crustal levels. The rifts on Iceland are separated from the Reykjanes Ridge to the south and the Kolbeinsey Ridge to the north by large transform faults. This precludes communication of melt from central Iceland to these ridges north and south. If the plume only feeds crustal formation between these transform faults, the crust along the Reykjanes Ridge must be generated by more normal, passive upwelling and decompressional melting. This is likely as the crustal thicknesses observed (12 to 16 km) could be generated by passive upwelling of warm mantle with a potential temperature range of 1370 to 1430°C [*Weir et al.*, 2001]. We therefore suggest that melting in the plume core feeds crustal generation on Iceland between the transforms to the north and south. Plume source material, however, spreads over much greater distances providing warm mantle with a plume isotopic signature for crustal generation along the Reykjanes Ridge. Given this model, we calculate a crustal generation rate from the plume of 0.2 km^3/yr.

[51] This crustal generation rate is only 8% of the plume volume flux which is considerably lower than the estimated degree of partial melting of 20–30% based on basalt compositions on Iceland [*White et al.*, 1995; *White and McKenzie*, 1995]. In order for the percentage melt to reach 20–30% in the plume melt zone, two thirds of the plume flux must not melt at all leaving only the remaining third to melt up to 20–30%. This implies that the bulk of the fertile plume material flows laterally away from Iceland without any melting. The proportion of plume material participating in the melting process beneath Iceland is probably even smaller than this one third estimate as our estimate of plume volumetric flux is a minimum. In estimating the plume flux of 2.5 km^3/yr we assumed that the velocity of the asthenospheric layer is everywhere less than the plate separation rate. The range of crustal thickness (15–46 km) in Iceland imply that material is being fluxed through the melt zone beneath central Iceland between 1 and 3 times the rate that would be expected for passive isentropic upwelling. We would therefore expect plume material to flow away from the melting zone at a rate greater than the plate spreading rate. This would increase the plume volumetric flux estimate.

[52] These arguments imply that (1) the plume is fluxing material through the melt zone beneath Iceland in order to produce crust as thick as observed, and (2) the bulk of plume material does not participate in melting beneath Iceland and is thus presumably transported horizontally away, perhaps feeding the mantle low-velocity zone. This observation is similar to that made by *Davies* [1999] for the Hawaii plume. He estimates that perhaps 80–90% of the plume does not melt at all.

7. Summary

[53] 1. The combination of teleseismic body wave data with surface wave phase velocity measurements allows improved tomographic imaging of the upper mantle beneath Iceland including recovery of absolute velocities. Using the 3-D crustal velocity model for Iceland ICECRTb [*Allen et al.*, 2002], we remove the crustal signal allowing improved resolution of uppermost mantle velocity anomalies, the region of plume-ridge interaction.

[54] 2. A vertical cylindrical low-velocity anomaly extends from a depth of at least 400 km up to a depth of ~200 km, a geometry consistent with a mantle plume feeding high-temperature material toward the surface. The anomaly has a radius of 60–100 km. The best estimates of maximum velocity anomaly we obtain from this travel time tomographic study are −3.8% for V_S and −2.1% for V_P which are consistent with the anomaly expected given a plume with an excess temperature in the 140–260 K range as predicted by geochemical estimates. It must be noted, however, that wave front healing effects not accounted for in this study may mean the velocity anomalies are much higher e.g. −12% for V_S [*Allen et al.*, 1999].

[55] 3. Above 200–250 km depth the nature of the velocity anomaly changes significantly. Combination of the relative velocities with an absolute average velocity for Iceland suggests this change is due to the presence of a horizontal low-velocity plume head in this depth range.

[56] 4. Within the plume head we resolve relatively high velocities in both V_P and V_S in the uppermost mantle (above 100 km depth) above the plume core and beneath the thickest crust in central Iceland. We suggest that these anomalies are the result of higher degrees of partial melt in the plume today compared to the last ~20 Myr which is expected given the plume is at its most active for the same time period.

[57] 5. Comparison of the plume volumetric flux with the crustal generation flux suggests a maximum of 8% melting in the mantle beneath Iceland. This is less than the estimated 15–20% melting beneath normal mid-ocean ridges and the 20–30% melting calculated from REE Inversions of basalt compositions in Iceland. The discrepancy is reconciled if only a third of plume material passes through the melt zone. This, in turn, would suggest that a significant proportion of the fertile mantle plume does not pass through the melt zone beneath Iceland but is instead transported away in the plume head.

[58] **Acknowledgments.** This work was funded by NSF EAR/9417918 and NERC GST/02/1238. We would like to thank Tony Dahlen for regular discussions, Paul Friberg and Sid Hellman from the IRIS–PASSCAL project for their support in the field and data handling operations, and all the Icelanders who lodged our instruments. We also thank Frederik Tilmann and Rob van der Hilst for reviewing the manuscript. The figures were produced with GMT [*Wessel and Smith*, 1995].

References

Allen, R. M., G. Nolet, W. J. Morgan, K. Vogfjörd, B. H. Bergsson, P. Erlendsson, G. R. Foulger, S. Jakobsdóttir, B. R. Julian, M. Pritchard, S. Ragnarsson, and R. Stefánsson, The thin hot plume beneath Iceland, *Geophys. J. Int.*, *137*, 51–63, 1999.

Allen, R. M., G. Nolet, W. J. Morgan, K. Vogfjörd, M. Nettles, G. Ekström, B. H. Bergsson, P. Erlendsson, G. R. Foulger, S. Jakobsdóttir, B. R. Julian, M. Pritchard, S. Ragnarsson, and R. Stefánsson, Plume-driven plumbing and crustal formation in Iceland, *J. Geophys. Res.*, *107*(B8), 2163, doi:10.1029/2001JB000584, 2002.

Anderson, D. L., The statistics of helium isotopes along the global spreading ridge system and the central limit theorem, *Geophys. Res. Lett.*, *27*, 2401–2404, 2000.

Bijwaard, H., and W. Spakman, Tomographic evidence for a narrow whole mantle plume below Iceland, *Earth Planet. Sci. Lett.*, *166*, 121–126, 1999.

Bjarnason, I. T., W. Menke, O. G. Flovenz, and D. Caress, Tomographic image of the Mid- Atlantic plate boundary in southwestern Iceland, *J. Geophys. Res.*, *98*, 6607–6622, 1993.

Bjarnason, I.-T., C.-J. Wolfe, S.-C. Solomon, and G. Gudmundson, Initial results from the ICEMELT experiment: Body-wave delay times and shear-wave splitting across Iceland, *Geophys. Res. Lett.*, *23*, 459–462, 1996.

Darbyshire, F. A., I. T. Bjarnason, R. S. White, and O. G. Flovenz, Crustal structure above the Iceland mantle plume imaged by the ICEMELT refraction profile, *Geophys. J. Int.*, *135*, 1131–1149, 1998.

Darbyshire, F. A., K. F. Priestley, R. S. White, R. Stefansson, G. B. Gudmundsson, and S. S. Jakobsdottir, Crustal structure of central and northern Iceland from analysis of teleseismic receiver functions, *Geophys. J. Int.*, *143*, 163–184, 2000a.

Darbyshire, F. A., R. S. White, and K. F. Priestley, Structure of the crust and uppermost mantle of Iceland from a combined seismic and gravity study, *Earth Planet. Sci. Lett.*, *181*, 409–428, 2000b.

Davies, G. F., *Dynamic Earth: Plates, Plumes and Mantle Convection*, 458 pp., Cambridge Univ. Press, New York, 1999.

DeMets, C., R. G. Gordon, D. F. Argus, and S. Stein, Effect of recent revisions to the geomagnetic reversal time-scale on estimates of current plate motions, *Geophys. Res. Lett.*, *21*, 2191–2194, 1994.

Dziewonski, A. M., and D. L. Anderson, Preliminary Reference Earth Model, *Phys. Earth Planet. Inter.*, *25*, 297–356, 1981.

Engdahl, E. R., R. D. van der Hilst, and R. Buland, Global teleseismic earthquake relocation with improved travel times and procedures for depth determination, *Bull. Seismol. Soc. Am.*, *88*, 722–743, 1998.

Foulger, G. R., M. J. Pritchard, B. R. Julian, J. R. Evans, R. M. Allen, G. Nolet, W. J. Morgan, B. H. Bergsson, P. Erlendsson, S. Jakobsdóttir, S. Ragnarsson, R. Stefansson, and K. Vogfjörd, The seismic anomaly beneath Iceland extends down to the mantle transition zone and no deeper, *Geophys. J. Int.*, *142*, F1–F5, 2000.

Hardarson, B. S., J. G. Fitton, R. M. Ellam, and M. S. Pringle, Rift relocation–A geochemical and geochronological investigation of a palaeo-rift in northwest Iceland, *Earth Planet. Sci. Lett.*, *153*, 181–196, 1997.

Helmberger, D. V., L. Wen, and X. Ding, Seismic evidence that the source of the Iceland hotspot lies at the core-mantle boundary, *Nature*, *396*, 251–255, 1998.

Hung, S. H., F. A. Dahlen, and G. Nolet, Frechet kernels for finite-frequency traveltimes, II, Examples, *Geophys. J. Int.*, *141*, 175–203, 2000.

Isaak, D. G., High-temperature elasticity of iron-bearing olivines, *J. Geophys. Res.*, *97*, 1871–1885, 1992.

Ito, G., J. Lin, and C. W. Gable, Dynamics of mantle flow and melting at a ridge-centered hotspot; Iceland and the Mid-Atlantic Ridge, *Earth Planet. Sci. Lett.*, *144*, 53–74, 1996.

Jordan, T. H., Mineralogies, densities and seismic velocities of garnet lherzolites and their geophysical implications, in *The Mantle Sample: Inclusions in Kimberlites and Other Volcanics*, edited by F. R. Boyd and H. O. Meyer, pp. 1–14, AGU, Washington, D.C., 1979.

Karato, S., Importance of anelasticity in the interpretation of seismic tomography, *Geophys. Res. Lett.*, *20*, 1623–1626, 1993.

Kennett, B. L. N., and E. R. Engdahl, Traveltimes for global earthquake location and phase identification, *Geophys. J. Int.*, *105*, 429–465, 1991.

Kincaid, C., G. Ito, and C. Gable, Laboratory investigation of the interaction of off-axis mantle plumes and spreading centres, *Nature*, *376*, 758–761, 1995.

Magde, L. S., A. H. Barclay, D. R. Toomey, R. S. Detrick, and J. A. Collins, Crustal magma plumbing within a segment of the Mid-Atlantic Ridge, 35°N, *Earth Planet. Sci. Lett.*, *175*, 55–67, 2000.

McKenzie, D., The generation and compaction of partially molten rock, *J. Petrol.*, *25*, 713–765, 1984.

McKenzie, D., Constraints on melt generation and transport from U-series activity ratios, *Chem. Geol.*, *162*, 81–94, 2000.

Menke, W., M. West, B. Brandsdottir, and D. Sparks, Compressional and shear velocity structure of the lithosphere in Northern Iceland, *Bull. Seismol. Soc. Am.*, *88*, 1561–1571, 1998.

Morgan, W. J., Convection plumes in the lower mantle, *Nature*, *230*, 42–43, 1971.

Nataf, H. C., Seismic imaging of mantle plumes, *Annu. Rev. Earth Planet. Sci.*, *28*, 391–417, 2000.

Navin, D. A., C. Peirce, and M. C. Sinha, The RAMESSES experiment, II, Evidence for accumulated melt beneath slow spreading ridge from wide-angle refraction and multichannel reflection seismic profiles, *Geophys. J. Int.*, *135*, 746–772, 1998.

Nishimura, C. E., and D. W. Forsyth, The anisotropic structure of the upper mantle in the pacific, *Geophys. J.*, *96*, 203–229, 1989.

Nolet, G., Partitioned waveform inversion and two-dimensional structure under the network of autonomously recording seismographs, *J. Geophys. Res.*, *95*, 8499–8512, 1990.

Nolet, G., and F. A. Dahlen, Wave front healing and the evolution of seismic delay times, *J. Geophys. Res.*, *105*, 19,043–19,054, 2000.

Paige, C. C., and M. A. Saunders, LSQR—An algorithm for sparse linear-equations and sparse least-squares, *ACM Trans. Math. Software*, *8*, 43–71, 1982.

Priestley, K., and F. Tilmann, Shear-wave structure of the lithosphere above the Hawaiian hot spot from two-station Rayleigh wave phase velocity measurements, *Geophys. Res. Lett.*, *26*, 1493–1496, 1999.

Ribe, N. M., The dynamics of plume-ridge interaction, 2, Off-ridge plumes, *J. Geophys. Res.*, *101*, 16,195–16,204, 1996.

Riley, G. N., and D. L. Kohlstedt, Kinetics of melt migration in upper mantle-type rocks, *Earth Planet. Sci. Lett.*, *105*, 500–521, 1991.

Ritsema, J., H. J. van Heijst, and J. H. Woodhouse, Complex shear wave velocity structure imaged beneath Africa and Iceland, *Science*, *286*, 1925–1928, 1999.

Sato, H., I. S. Sacks, T. Murase, G. Muncill, and H. Fukuyama, Attenuation of compressional waves in peridotite measured as a function of temperature at 200 MPa, *Pure Appl. Geophys.*, *128*, 433–447, 1988.

Schilling, J. G., Fluxes and excess temperatures of mantle plumes inferred from their interaction with migrating midocean ridges, *Nature*, *352*, 397–403, 1991.

Shen, Y., S. C. Solomon, I. T. Bjarnason, and C. J. Wolfe, Seismic evidence for a lower-mantle origin of the Iceland plume, *Nature*, *395*, 62–65, 1998.

Shen, Y., S. C. Solomon, I. T. Bjarnason, G. Nolet, W. J. Morgan, R. M. Allen, K. Vogfjord, S. Jakobsdottir, R. Stefansson, G. F. Foulger, and B. Julian, Seismic evidence for a tilted mantle plume and large-scale, north-south flow beneath Iceland, *Earth Planet. Sci. Lett.*, *197*, 261–272, 2002.

Sleep, N.-H., spots and mantle plumes: Some phenomenology, *J. Geophys. Res.*, *95*, 6715–6736, 1990.

Staples, R. K., R. S. White, B. Brandsdottir, W. Menke, P. K. H. Maguire, and J. H. McBride, Faroe-Iceland Ridge Experiment, 1, Crustal structure of northeastern Iceland, *J. Geophys. Res.*, *102*, 7849–7866, 1997.

Stefansson, R., R. Bodvarsson, R. Slunga, P. Einarsson, S. Jakobsdottir, H. Bungum, S. Gregersen, J. Havskov, J. Hjelme, and H. Korhonen, Earthquake prediction research in the South Iceland Seismic Zone and the SIL project, *Bull. Seismol. Soc. Am.*, *83*, 696–716, 1993.

Tryggvason, K., E. S. Husebye, and R. Stefansson, Seismic image of the hypothesized Icelandic hot spot, *Tectonophysics*, *100*, 97–118, 1983.

VanDecar, J. C., and R. S. Crosson, Determination of teleseismic relative phase arrival times using multi-channel cross-correlation and least squares, *Bull. Seismol. Soc. Am.*, *80*, 150–169, 1990.

Weir, N. R. W., R. S. White, B. Brandsdottir, P. Einarsson, H. Shimamura, H. Shiobara, and R. F. Team, Crustal structure of the northern Reykjanes Ridge and the Reykjanes Peninsula, southwest Iceland, *J. Geophys. Res.*, *106*, 6347–6368, 2001.

Wessel, P., and W. H. F. Smith, New version of the Generic Mapping Tools released, *Eos. Trans. AGU*, *76*, 329, 1995.

White, R. S., Rift-plume interaction in the North Atlantic, *Philos. Trans. R. Soc. London, Ser. A*, *355*, 319–339, 1997.

White, R. S., and D. McKenzie, Mantle plumes and flood basalts, *J. Geophys. Res.*, *100*, 17,543–17,585, 1995.

White, R. S., J. W. Bown, and J. R. Smallwood, The temperature of the Iceland plume and origin of outward-propagating V-shaped ridges, *J. Geol. Soc.*, *152*, 1039–1045, 1995.

Wielandt, E., On the validity of the ray approximation for interpreting delay times, in *Seismic Tomography; With Applications in Global Seismology and Exploration Geophysics*, edited by G. Nolet, pp. 85–98, D. Reidel, Norwell, Mass., 1987.

Wolfe, C.-J., I.-T. Bjarnason, J.-C. VanDecar, and S.-C. Solomon, Seismic structure of the Iceland mantle plume, *Nature*, *385*, 245–247, 1997.

Zhao, D., structure and origins of hotspots and mantle plumes, *Earth Planet. Sci. Lett.*, *192*, 251–265, 2001.

R. M. Allen, Department of Geology and Geophysics, University of Wisconsin–Madison, 1215 W. Dayton St., Madison, WI 53706, USA. (rallen@geology.wisc.edu)

B. Bergsson, P. Erlendsson, S. Jakobsdóttir, S. Ragnarsson, R. Stefánsson, and K. Vogfjörd, Vedurstofa Íslands, Bústadavegur 9, 150 Reykjavík, Iceland.

G. Foulger and M. Pritchard, Department of Geological Sciences, University of Durham, Science Laboratories, South Road, Durham DH1 3LE, UK.

B. Julian, U.S. Geological Survey, 345 Middlefield Road, MS 977, Menlo Park, CA 94025, USA.

W. J. Morgan and G. Nolet, Department of Geosciences, Guyot Hall, Princeton University, Princeton, NJ 08544, USA. (wjmorgan@princeton.edu; nolet@princeton.edu)